Environmental Science Water Research & Technology



PAPER

View Article Online
View Journal | View Issue



Cite this: Environ. Sci.: Water Res. Technol., 2021, 7, 521

Low concentrations of Cu²⁺ in synthetic nutrient containing wastewater inhibit MgCO₃-to-struvite transformation

Karolina Barčauskaitė, ^{Dab} Donata Drapanauskaitė, ^{ab} Manoj Silva, ^{Da} Vadim Murzin, ^{cd} Modupe Doyeni, ^b Marius Urbonavicius, ^e Clinton F. Williams, ^{Df} Skaidrė Supronienė ^{Db} and Jonas Baltrusaitis ^{D*a}

Simultaneous major nutrient nitrogen (N) and phosphorus (P) recovery from wastewater is key to achieving food–energy–water sustainable development. In this work, we elucidate the reaction kinetics, crystalline structure and chemical composition of the resulting solid precipitate obtained from simulated N and P containing wastewater solution using widely abundant low solubility magnesite (MgCO₃) particles in the presence of common transition metal ions, such as zinc (Zn²⁺) or copper (Cu²⁺). We show that up to 100 ppm Zn²⁺ from the simulated wastewater can be incorporated into the struvite lattice as isolated distorted Zn²⁺ while even at very low concentrations of ~5 ppm Cu²⁺ ions almost completely inhibit struvite crystal formation. The resulting solid precipitate distinctly affects soil microbial biomass carbon and soil dehydrogenase enzyme activity. These results show a cautionary case where abundant natural mineral MgCO₃ exhibits very different chemistry in Cu²⁺ containing simulated wastewater and does not readily adsorb or retain NH₄⁺ and PO₄³⁻ ions, unlike less sustainable but more water-soluble magnesium sources, such as MqCl₂, at the equivalent [Mg²⁺]: [NH₄⁺]: [PO₄³⁻] molar ratio of 1.4:1:1.

Received 24th November 2020, Accepted 28th December 2020

DOI: 10.1039/d0ew01035a

rsc.li/es-water

Water impact

Recovering nutrients from wastewater is an emerging field of interest due to the impact modern agriculture has on aquatic ecosystems. This work presents the impact of transition metals (Cu and Zn which are common contaminants in municipal and industrial wastewater) being present at the heterogeneous interface of struvite crystallization ($MgNH_4PO_4$ - $6H_2O$) on magnesite ($MgCO_3$).

Introduction

Modern agricultural practices and the increasing use of mineral fertilizers have significantly perturbed the global nitrogen (N) and phosphorus (P) cycles. Due to soil bacteria activity, a loss of up to 90% of the applied N can take place. Concomitantly, ammonia synthesis using air N₂ requires 4% of the world's annual natural gas supply as well as 1% of the annual global energy production. P, on the

other hand, is mined from rock and it is dwindling without replenishment.^{5,6} P fertilizers are much less water-soluble and enter the watershed *via* runoff.⁷ Therefore, producing green fertilizer materials that are more stable in the environment becomes important in promoting sustainable agricultural practices.⁸⁻¹¹ Specifically, producing fertilizers containing both N and P from wastewater streams is an important aspect of sustainable development.

Struvite (MgNH₄PO₄·6H₂O) synthesis is a unique opportunity that allows for the simultaneous removal of both N-NH₄⁺ and P-PO₄³⁻ from wastewater streams. It is a low solubility fertilizer that is more environmentally sustainable, compared to the conventional N fertilizers which have the propensity to volatilize and emit greenhouse gases. Struvite precipitation from wastewater so far has chiefly utilized soluble magnesium precursors, such as magnesium chloride (MgCl₂), which also require wastewater pH adjustment with external chemicals, such as NaOH. Earth-abundant low solubility magnesium sources, such as periclase (MgO), 10,16-18 magnesite (MgCO₃), 19,20 brucite (Mg(OH)₂), 21 and dolomite

^a Department of Chemical and Biomolecular Engineering, Lehigh University, B336 Iacocca Hall, 111 Research Drive, Bethlehem, PA 18015, USA. E-mail: job314@lehigh.edu; Tel: +1 610 758 6836

^b Lithuanian Research Centre for Agriculture and Forestry, Instituto al.1, LT-58344, Akademija, Kedainiai District, Lithuania

^c Bergische Universität Wuppertal, Gaußstraße 20, D-42119, Wuppertal, Germany ^d Deutsches Elektronen Synchrotron DESY, Notkestraße 85, D-22607 Hamburg, Germany

^e Center for Hydrogen Energy Technologies, Lithuanian Energy Institute, 3 Breslavios. 44403 Kaunas. Lithuania

^f USDA-ARS, US Arid Land Agricultural Research Center, 21881 N. Cardon Ln, Maricopa, AZ, 85138, USA

(CaMg(CO₃)₂), ^{13,22,23} have also been reported to form struvite from model wastewater containing NH₄⁺ and PO₄³⁻ albeit under distinctly different reaction kinetics.⁷⁷ Due to their alkaline nature, upon partial dissolution, they result in a solution pH increase and do not require addition of NaOH. However, anthropogenic wastewater has a complex chemical composition and contains transition metal ions originating from industrial, municipal and agricultural activities.²⁴ Copper (Cu) and zinc (Zn) are of particular interest given their presence in sewage sludge from domestic and industrial wastewater, which is often a feedstock of interest for nutrient capture since it is rich in N and P.25 Studies have reported Cu2+ and Zn2+ concentrations in municipal wastewater from 10-90 ppb to 49-498 ppb, respectively.²⁶ However, sewage sludge obtained from mixed domestic and industrial wastewater averaged 1700 ppm of Zn and 500 ppm of Cu²⁺, 27 while the sewage sludge of a municipal stormwater treatment plant contained up to 500 ppm of Zn²⁺ and 50 ppm of Cu²⁺. These relatively low concentrations of Cu²⁺ and Zn²⁺ were shown to not result in significant struvite morphological changes when using MgCl₂, despite the kinetic hindering effects.²⁹ Structurally, Zn²⁺ can be incorporated into the solid precipitate crystal lattice or sorbed on the surface during struvite precipitation from separated sewage sludge anaerobic digester effluent using MgCl2 reducing the purity of the solid precipitate. 30-34 Previous studies on struvite synthesis using MgCl2 in the presence of Zn²⁺ and Cu²⁺ aqueous ions have also shown that these metals are incorporated into the struvite as phosphate and hydroxide phases. 32-34 For example, Peng et al. demonstrated that in the presence of Cu²⁺ concentrations from 200 ppm to 800 ppm Cu(OH)2 was formed in addition to struvite.35 Rouff et al. investigated the structure of these metals in synthesized struvite using MgCl2 and found polymeric Zn units even at low concentrations.32 Further studies by the same authors showed that Cu²⁺ was also incorporated into the struvite structure, but was affected by the organic matter content in the wastewater.³³ Notably, water-soluble MgCl2 was predominantly used and the effects of Zn2+ and Cu2+ on the struvite formation kinetics and the resulting crystal structure using low solubility Mg minerals were not largely studied. While some reports have claimed that struvite formed from wastewater does not contain significant heavy metal concentrations, 36 it is now evident that the concentration of metals in wastewater plays an important role and can result in significant adsorption into the solid struvite^{33,34} which can have detrimental effects on soil biota.

The accumulation and bioavailability of heavy metals in the food chain depend on various environmental factors such as temperature and physicochemical properties of the soil such as organic matter content, pH, and cationic exchange capacity.37 This work aims to investigate the effects of Cu2+ and Zn2+ on the struvite formation kinetics from simulated wastewater and product distribution using low solubility magnesium-containing minerals, such as MgCO₃, rather than water-soluble salts, such as MgCl2, as well as struvite effects on soil biome. In particular, studies were performed to assess the impact of Cu²⁺ and Zn²⁺ incorporated struvite synthesized

using MgCO3 on dehydrogenase activity (DHA) and soil microbial biomass carbon (SMBC) in soil. The unexpected soil biota testing results were further elucidated by investigating the struvite formation reaction kinetics using ion chromatography to assess NH₄⁺ and PO₄³⁻ ion removal from simulated wastewater solution while the resulting Cu²⁺ and Zn2+ concentrations in the solid precipitate were measured using inductively coupled plasma mass spectroscopy (ICP-MS). The resulting struvite crystalline structure was analyzed using powder X-ray diffraction (XRD), and the particle morphology and elemental analysis were obtained using electron microscopy (SEM/EDS) while the atomic information on the structure of the metals was probed using X-ray absorption spectroscopy (XAS).

Experimental methods

Reagents and solutions

Magnesium carbonate (MgCO₃) (magnesite), magnesium as MgO ≥40% and monoammonium phosphate (NH₄H₂PO₃) ≥98% were purchased from Sigma-Aldrich. Copper(II) nitrate trihydrate $(Cu(NO_3)_2 \cdot 3H_2O) \ge 99.5\%$ and nitric acid (HNO_3) 65% were obtained from Merck. Zinc nitrate hexahydrate (Zn(NO₃)₂·6H₂O) 98% was obtained from Acros Organics.

Struvite synthesis

The synthesis procedure is shown in Fig. 1. In particular, struvite synthesis from simulated wastewater was performed using the low solubility abundant magnesite mineral. Cuand Zn-containing struvites were synthesized using copper(II) nitrate trihydrate and zinc(II) nitrate hexahydrate. A stock solution containing 1000 ± 1 ppm of monoammonium phosphate (NH₄H₂PO₄) was used. The weighed solid Cu²⁺ or Zn²⁺ amounts were added into the prepared 1000 ppm MAP solution to result in the final concentrations of 2 \pm 0.02, 5 \pm 0.05, 10 \pm 0.1 or 20 \pm 0.2 ppm for Cu²⁺ and 100 \pm 0.5 ppm for Zn²⁺ with constant stirring at 400 rpm. 1000 ppm MAP represents PO43- and NH4+ values found in municipal, animal and industrial wastewater38 while maintaining above the 1:1 molar ratio needed for struvite formation. Finally, MgCO₃ powder was added at 1000 ppm concentration to the simulated wastewater and stirred for up to 120 minutes. The total volume of the reactive solution was 750 mL. 1.5 mL of solution was sampled periodically and filtered through a 25 mm nylon filter (0.45 µm size) to remove the solid precipitate. The filtrate was diluted 5 times with 2% HNO₃ and analyzed by ICP-MS for Zn and Cu content and residual Mg^{2+} , PO_4^{3-} and NH_4^+ ions using IC.

Ion chromatography

A Shimadzu HIC-20A Super ion chromatography system (Kyoto, Japan) was used in all experiments to measure Mg²⁺, NH₄⁺ and PO₄³⁻ ions. The separation columns used were Shim-pack IC-SC1 (4.6 × 150 mm) with Guard column Shimpack IC-SC1 (G) (4.6 × 10 mm) for cation analysis and Shim-

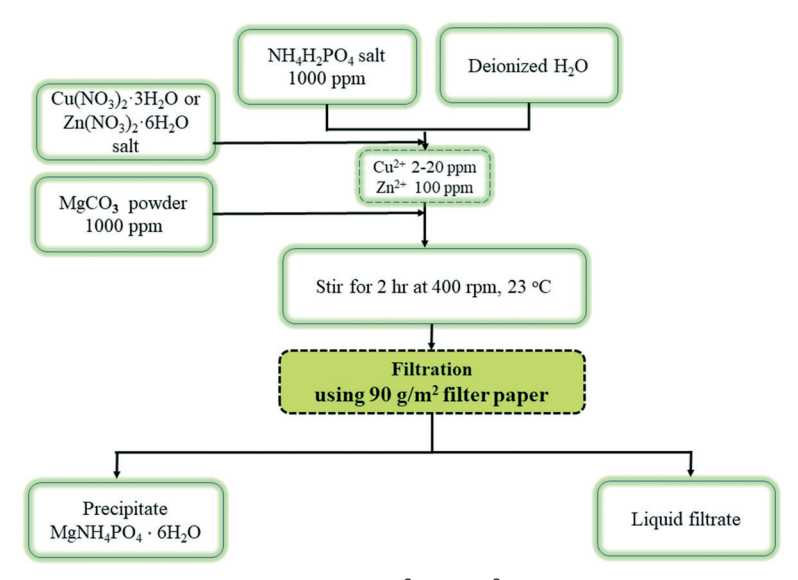


Fig. 1 Experimental procedure for struvite synthesis with and without Cu^{2+} and Zn^{2+} in simulated wastewater.

pack IC-SA2 (4.0 × 250 mm) with Guard column Shim-pack SA2 (G) $(4.6 \times 10 \text{ mm})$ for anion analysis. The sample-loop volume was 1000 µL in the cation and anion systems and eluted species were measured using an electrical conductivity detector CDD-10ASP. 1.8 nM Na₂CO₃/1.7 mM NaHCO₃ was used as eluent for anion analysis while 0.7 mM methanesulfonic acid for cation analysis. All samples were measured at room temperature. The system was computercontrolled through LabSolution software. Error bars represent uncertainty from three independent measurements.

Inductively coupled plasma mass spectrometry (ICP-MS) analysis

Solid precipitate samples were digested using microwaveassisted extraction (MAE) by means of a CEM MARS 6® (Matthews, NC, USA) digestion system equipped with a 100 mL Teflon vessel. Approximately, 0.1 g of solid struvite sample was accurately weighed into a Teflon vessel and digested using 10 mL of analytical grade concentrated nitric acid (≥65%) (Sigma-Aldrich, Germany). Before digestion, the samples were soaked in acid for 30 min at room temperature. Digestion was performed under the following conditions: temperature - 200 °C; pressure - 800 psi; ramp time - 15 min; hold time - 20 min; microwave power - 1600 W. The digested samples were cooled down and thoroughly transferred into a 100 mL volumetric flask and diluted using bidistilled water till the mark. The blank sample was included in each digestion run. To measure concentrations of Mg, P, Cu and Zn an inductively coupled plasma mass spectrometer (ICP-MS) was operated in standard mode. The samples were introduced from an autosampler incorporating an ASXpress™ rapid uptake module (Cetac ASX-520, Teledyne Technologies Inc., USA) through a PEEK nebulizer (Burgener Mira Mist, Mississauga, Burgener Research Inc., Canada). The analyzed elements were estimated using an external multi-element six-point calibration curve in the range of 50-2000 ppb (50, 100, 200, 500, 1000, 2000 ppb). The standard mixture solution of multiple microelements (Mg, P, Cu, Zn) in 2% nitric acid was obtained from CPAchem (Bulgaria). Double distilled water was obtained using a distillation apparatus (Thermo Scientific, USA) and used for dilution in all cases.

Powder X-ray diffraction

The crystal structure of the samples was analyzed via the X-ray diffraction (XRD) method using a Bruker D8 diffractometer (40 kV, 40 mA) operated in the θ - θ configuration. The measurements were performed at 2θ angle in the scan range of 20–70° using Cu cathode K α radiation (λ = 0.15406 nm) in steps of 0.01° and a Lynx eye position-sensitive detector.

Scanning electron microscopy

The morphology of the struvite surface was examined with a scanning electron microscope (SEM, Hitachi S-3400N) using a secondary electron detector at an accelerating voltage of 3 kV. Energy-dispersive X-ray spectroscopy (EDS, Bruker Quad 5040) was used for the analysis of the elemental mapping of the samples.

X-ray absorption near edge spectroscopy (XANES) and extended X-ray absorption fine structure (EXAFS)

X-ray absorption near edge spectroscopy (XANES) and extended X-ray absorption fine structure (EXAFS) measurements were performed at the advanced X-ray absorption spectroscopy beamline P64 (PETRA III ring, DESY, Hamburg).³⁹ The samples were mixed with microcrystalline cellulose and pressed into powder pellets. The spectra were measured at room temperature in continuous acquisition mode when the undulator and the monochromator movements were synchronized on the fly. Three ionization chambers were filled with pure nitrogen to reduce the sensitivity to higher

harmonics of the undulator. For each set of samples, the corresponding metal foil (Cu or Zn) was used as a standard between the second and the third ionization chambers. The monochromatic beam flux on the sample was ca. 5×10^{12} photons per s. The time for each spectrum was set to 5 minutes; an average of 3-4 scans was used for the analysis.

The experimental EXAFS spectra were fitted using IFEFFIT and LARCH packages. 40,41 In the fitting procedure ab initio photoelectron backscattering amplitudes and phases were calculated self-consistently using the FEFF8.5 code.42 The EXAFS functions were k^2 - and k^3 -weighted and fitted in a 1.0-3.0 Å interval of R-space. The range of photoelectron wave vectors used in the fit was 3.0-15.0 Å⁻¹. The amplitude reduction factor S_0^2 was obtained from the fit of the first shell of the corresponding standard (0.87 for Cu, 0.85 for Zn). Coordination numbers were fixed, different models with different coordination numbers were tested, and the best model and fit were taken. The Debye-Waller factors, σ^2 , distances, R, and the total energy shift, ΔE_0 , were varied during the fit.

Soil microbial biomass activity measurements

The soil was collected from the experimental field site at the Institute of Agriculture, Lithuania Research Centre for Agriculture and Forestry (55°40' N, 23°87' E). The soil was Endocalcari-Epihypogleyic Cambisol characterized by a homogeneous texture. Soil samples (0-20 cm) were collected and visible plant debris, soil animals and stones were manually removed from the field moist soil samples. The remaining soil was thoroughly mixed, air-dried at room temperature, passed through a 2 mm sieve and adjusted to 40% water holding capacity (WHC) by adding deionized water.

The soil was introduced into polyvinyl chloride trapezoidal-section containers (chemically inert and opaque to light) of approximately 1 L capacity and the soil layer was separated from the container using a paper mesh. To evaluate the struvite effect on the soil microorganism activity and microbial biomass content, pots with soil and struvite synthesized using various precursors were stored under controlled climate conditions in laboratory incubators (CLIMACELL 707, MMM Medcenter Einrichtungen GmbH, Munich, Germany). The laboratory incubator parameters were set for a day and night mode as follows: temperature -23 \pm 0.5 °C during the day and 18 \pm 0.5 °C during the night, RH - 68 \pm 2%, fan mode on 100%, light on during the day and light off during the night. Deionized water was regularly added to the pots to maintain the water content at 40% WHC. Soil samples for soil dehydrogenase enzyme activity and soil microbial biomass carbon determination were taken after 0, 5, 28 and 48 days. The measured organic carbon content was 1.30 \pm 0.15%, the total N was 0.14 \pm 0.02%, and the P_2O_5 and K_2O concentrations were 134.00 \pm 6.56 mg kg⁻¹ and 142.67 mg kg⁻¹, respectively. The measured pH was 7.03 \pm 0.15. The soil contained 4139 \pm 955 mg kg⁻¹ Ca and 947 \pm 258 mg kg⁻¹ Mg. Approximately 1000 g of soil was mixed with struvite and struvite synthesized using Cu2+ and Zn2+

precursors. The amount of struvite was calculated according to the Nitrates Directive (91/676/EEC) to obtain 170 kg of N per one hectare. The pot experiments were performed in triplicate with four amendments namely, control (soil without struvite), soil + struvite, soil + struvite which contains Zn²⁺ ions and soil + struvite which contains Cu²⁺ ions. The overview of the testing procedures is shown in Fig. 2.

Soil dehydrogenase enzyme activity (DHA) measurements

Dehydrogenase activity was determined according to the slightly modified method described earlier. 43 The collected soil samples were air-dried, homogenized and analyzed the same day. 20 g of air-dried soil and 0.2 g of CaCO3 were thoroughly mixed. 6 g each of this mixture was dispensed into three test tubes (three replicates of each sample). To each tube, 1 ml of 3% 2,3,5-triphenyltetrazolium chloride (TTC) aqueous solution and 2.5 ml distilled water were added. The contents of each tube were mixed with a glass rod and then the tube was stoppered and incubated at 37 °C for 24 hours. After 24 h, the stopper was removed, 10 ml methanol was added and the tube was shaken for 1 min using a vortex (IKA, Germany). The filtrate was transferred into a glass funnel and filtered to a 50 ml volumetric flask. The filtrate was diluted through the funnel to a 50 ml volume into the volumetric flask using methanol. The intensity of the red color was measured using a UV-vis spectrophotometer (Shimadzu, Japan) using a wavelength of 485 nm in a 1 cm cuvette with methanol as a blank reference. The amount of triphenyl formazan (TPF) produced by the soil samples was estimated using the calibration curve prepared using 5 to 50 µg ml⁻¹ TPF.

Soil microbial biomass carbon (SMBC) determination using the fumigation extraction method

SMBC was determined using the fumigation-extraction method. 44,45 20 g of soil was fumigated via exposing the soil to alcohol-free CHCl3 vapor in a sealed vacuum desiccator for 24 h. The fumigated soil was evacuated repeatedly in a clean empty desiccator until the odor of CHCl3 was no more detected and then extracted with 80 ml of 0.5 M K2SO4 (soil: $K_2SO_4 = 1:4$) for 30 min by oscillating shaking at 200 rpm and then filtered through Whatman No. 42 filter paper.

The organic carbon content in the extracts was measured using the dichromate digestion method. 2 ml of K₂Cr₂O₇ (66.7 mM) and 15 ml of the digestion mixture (2:1 conc. H₂-SO₄: H₃PO₄ (v/v)) were added to 8 ml of extract in a 250 ml conical flask. The mixture was gently refluxed for 30 min, allowed to cool and diluted with 20 ml distilled water. The excess K2Cr2O7 was measured by titration with ferrous ammonium sulfate (40.0 mM) using a 1,10-phenanthrolineferrous sulfate complex (25 mM) solution as an indicator. The extraction of non-fumigated soil was the same as that of the fumigated soil. SMBC was calculated from the differences in extractable organic carbon (OC) between the fumigated and non-fumigated soil samples with a conversion factor (KEC) of 0.38.44 SMBC was calculated as

Fig. 2 Experimental procedure for SMBC and DHA analysis

$$SMBC = Ec/KEC, (1)$$

where Ec = (OC extracted from fumigated soil) - (OC extracted from non-fumigated soil) and44

$$KEC = 0.38.$$
 (2)

Statistical analysis

Pairwise differences and analysis of variance (ANOVA) with Tukey's studentized range tests were calculated using the SAS program suite (SAS Institute Inc., USA). Pearson's correlation coefficients were used to investigate relationships between selected variables. Mean ± SE (standard error of the mean) was used to describe the variability of the measurements.

Results and discussion

Struvite synthesis and characterization

Kinetics of PO₄³⁻ and NH₄⁺ adsorption on MgCO₃ in the presence of Cu²⁺ and Zn²⁺. Struvite synthesis was performed using 1000 ppm MgCO3 and 1000 ppm MAP with and without 5 and 20 ppm Cu2+ and 100 ppm Zn2+ under otherwise identical conditions with no external pH adjustment. The concentrations of both metals were chosen to represent nutrient-containing wastewater to represent moderately contaminated sewage sludge. 27,28 The synthesized materials were dried at room temperature. The solid precipitate formed was analyzed for its crystalline structure, heavy metal content and local atomic coordination structure.

First, ion chromatography was used to monitor the timedependent anion (PO₄³⁻) and cation (NH₄⁺ and Mg²⁺) concentration change taking place in the liquid phase during the formation of the solid precipitate. Fig. 3a shows the concentration profile of residual PO₄³⁻ ions with an initial MgCO₃ concentration of 1000 ppm and 1000 ppm NH₄H₂PO₄ corresponding to a molar $[Mg^{2+}]$: $[NH_4^+]$: $[PO_4^{3-}]$ ratio of 1.4: 1:1. This was chosen after testing a wide range of initial MgCO₃ concentrations to efficiently supersaturate the solution to form struvite.19 The concentration profile of PO₄³⁻ showed a steep decrease in the presence of MgCO₃ alone and the presence of 100 ppm Zn²⁺. Notably, the reaction kinetics was completely inhibited for the 100 ppm Zn²⁺ case for at least 25 min after the reaction started, as evident via the plateau in the curve. Somewhat unexpectedly, virtually no change in the initial PO43- concentration was observed when 20 or 5 ppm Cu²⁺ was present. Only a notable decrease to ~600 ppm PO₄³⁻ was measured after 100 min in the presence of 5 ppm Cu2+ suggesting very slow reaction kinetics. MgCO₃ alone exhibited the fastest rate of PO₄³⁻ removal from solution, with a PO₄³⁻ concentration of 150 ppm at the equilibrium, after 2 hours. The time-resolved plot of the NH₄⁺ adsorption/reaction is shown in Fig. 3b. The NH₄⁺ adsorption and reaction with MgCO₃ followed a very similar behavior to that of PO43- with 5 and 20 ppm Cu2+ precursor solutions not removing any NH₄⁺ while MgCO₃ alone led to its complete removal. This suggests that a facile removal of both nutrient ions in the presence of 100 ppm Zn²⁺ is possible albeit exhibiting a delayed formation reaction for ~25 minutes. Important data are shown in the concentration profiles of Mg2+ in solution as a function of reaction time in Fig. 3c which showed that there was immediate dissolution (mobilization) of Mg²⁺ ions from solid

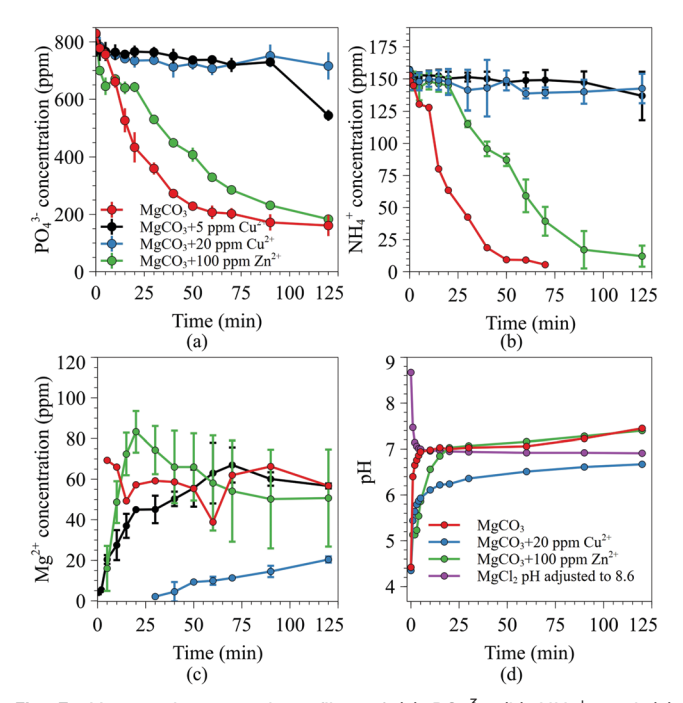


Fig. 3 Measured temporal profiles of (a) PO₄³⁻, (b) NH₄⁺, and (c) Mg²⁺ during struvite formation using 1000 ppm MgCO₃ and 1000 ppm MAP. (d) pH change as a function of reaction time, after addition of 1000 ppm MgCO₃ to 1000 ppm MAP. 5 and 20 ppm Cu²⁺ or 100 ppm Zn²⁺ were also used in simulated wastewater. In (d) the temporal pH profile of MgCl₂ with the initial pH adjusted to 8.6 is also shown for comparison. Error bars in (a)-(c) represent three independent measurements.

MgCO₃ within 5 min of the reaction. The initial fast dissolution was strongly inhibited in the 100 ppm Zn²⁺ case for 25 min and the same equilibrium concentration of Mg²⁺ ions was achieved. An increase in the Mg²⁺ ion concentration agreed well with the increasing pH of the solution as shown in Fig. 3d. Here the initial 1000 ppm NH₄H₂PO₄ solution pH was ~4.4 and the first measurement with MgCO₃ added was taken 1-2 min after the addition. Quite remarkable was the almost complete inhibition of Mg2+ ion release into solution when 20 ppm Cu²⁺ was present. Results show that while the pH increased in all the cases of MgCO3, the pH reached a steady-state value of \sim 7. While struvite formation typically requires a pH value of 8.5,12 the present experiments and literature data suggest that the bulk solution pH is not representative of the struvite formation conditions as the local pH on the MgCO₃ surface is likely higher. ¹⁹ Instead, low pH values of the solution should result in more dissolved Mg²⁺, the phenomenon not observed for the 20 ppm Cu²⁺ case. This suggests that the low concentration of Cu2+ ions inhibits the initial transformation, likely dissolution of Mg²⁺ ions, from the MgCO₃ surface necessary to form struvite, as opposed to the bulk solution pH driven transformations typically referred to in the literature. As supported by the XRD data (vide infra), 100 ppm Zn²⁺ containing NH₄H₂PO₄ solution precipitates as a zinc phosphate solid since its concentration is higher than that of Cu²⁺ and supersaturation

can be achieved for phosphate to be the most favorable solid phase, especially in the initial stage of the reaction. The Cu²⁺ concentrations used in these experiments do not lead to any detectable solid phases due to the absence of the supersaturation but rather Cu²⁺ ions adsorb on the MgCO₃ surface as Cu(OH)₂ blocking Mg²⁺ from being released into solution, a condition needed to form struvite, as shown in Fig. 3c. Importantly, a wide range of supporting experiments were performed using MgCl2 as a magnesium source at the molar amount equivalent to that of MgCO3 in the presence of 20 ppm Cu²⁺ and in all cases struvite formation was observed.

The kinetics of phosphate adsorption were analyzed using the pseudo-first order (PFO) and the pseudo-second order (PSO) models as shown in Fig. 4a and b, respectively. PSO is typically applicable when the adsorbing species represents one reactant and the surface site is the second reactant while in the PFO model the surface site is not part of the kinetic expression.46-48 Hence, literature reports which utilized MgCl₂ as the magnesium source reported that first-order kinetics can be used for struvite crystallization with no transition metal ions present. 49,50 Conceptually, however, phosphate adsorption on solid MgCO3 should follow PSO kinetics. However, previous reports that utilized MgCO3 for struvite synthesis have shown that the PFO model shows higher R^2 fits (with no transition metals present in aqueous solution), e.g. mathematically it is also correct even though lacking physical meaning.19 In this work, MgCO3 alone (no Cu²⁺ or Zn²⁺ present in the simulated wastewater solution) showed a higher R^2 value of 0.992 for the PFO model than that of 0.905 for PSO. One possible explanation for the PFO model showing high R^2 values compared to PSO in the case of phosphate adsorption on MgCO₃ could be that MgCO₃ has a higher solubility and thus, the surface restructuring steps required to adsorb phosphate may occur faster compared to adsorbents, such as MgO, 10,13,16,51 which exhibit true PSO type kinetic behavior. This is consistent with the data in Fig. 4a and kinetics data observed in Fig. 3c where Mg²⁺ is released into the bulk solution without Cu2+ or Zn2+ but at increasingly slower rates when 5 ppm Cu²⁺ or 100 ppm Zn²⁺ is present. The addition of 5 ppm and 20 ppm Cu²⁺ did not

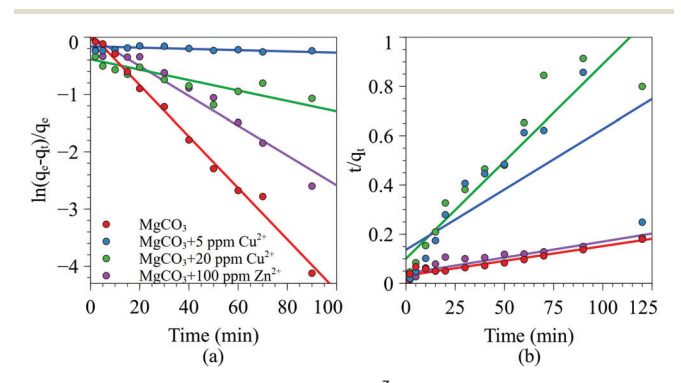


Fig. 4 Kinetic modeling of total PO₄³⁻ experimental data using (a) pseudo-1st order and (b) pseudo-2nd order kinetic models for 1000 ppm MgCO₃ and 1000 ppm MAP with and without 5 and 20 ppm Cu²⁺ or 100 ppm Zn²⁺.

result in high R^2 values, but due to the low phosphate adsorption as shown in Fig. 3a, this can be proposed due to the lack of struvite formation. 100 ppm of Zn²⁺ resulted in a satisfactory R2 value of 0.958 using both PFO and PSO kinetics. Hence, 100 ppm Zn²⁺ modified the reaction kinetics but did not inhibit struvite formation. Completely different was the measured reaction kinetics in the presence of either 20 or 5 ppm of Cu²⁺ which resulted in either poor PFO or PSO fits. This suggested a significant inhibition effect of ppm concentrations of Cu2+ when MgCO3 was used as a magnesium source. In contrast, literature reports showed that struvite crystallized in the presence of 5 ppm Cu²⁺ using $MgCl_2$ with the reported first-order rate constant of 3.58 h⁻¹, which showed that Cu²⁺ even at low concentrations inhibited struvite crystallization kinetics and an appreciable amount of solid struvite formed.²⁹ Interestingly, the same study²⁹ reported on struvite crystallization from MgCl2 in the presence of Zn²⁺, which showed similar results to Cu²⁺ where at a low concentration of 5 ppm, the reaction rates were similarly inhibited.

The Cu²⁺ and Zn²⁺ concentrations were measured as a function of time to understand the kinetics of metal adsorption on the solid phase and are shown in Fig. 5a. Typically, metal ion adsorption from wastewater follows PSO kinetics. 52-54 Therefore, the concentration data for Cu²⁺ and Zn²⁺ were fitted to the PSO model as shown in Fig. 5b. 5 and 20 ppm Cu²⁺ and 100 ppm Zn^{2+} experiments all fit the PSO model with R^2 values above 0.99, indicating that the PSO model is the correct approach to modeling the metal adsorption regardless of the concentration or metal nature. This suggests that metal ions adsorb on the heterogeneous MgCO3 (even though they were also recently shown to be efficiently adsorbed by struvite³⁴) surface with ~80% within the first 20 min of the reaction, suggesting that the observed plateau in Fig. 3a and b for both PO₄³⁻ and NH₄⁺ in the 100 ppm Zn²⁺ case is an initial reaction phase, likely through a solid zinc-containing intermediate. Similarly, the fast initial adsorption of Cu²⁺ suggests not the gradual incorporation into the lattice but rather the fast

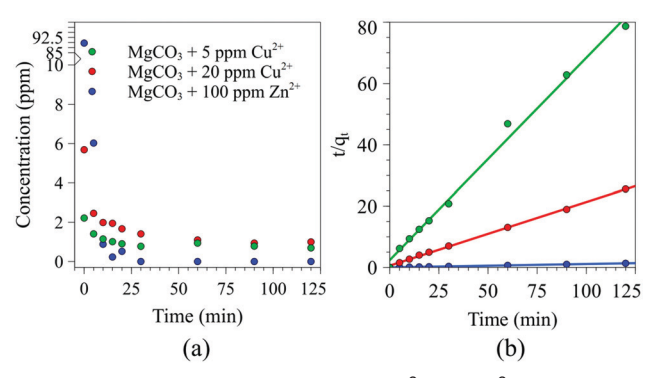


Fig. 5 (a) Measured temporal profiles of Cu²⁺ and Zn²⁺ during struvite formation using 1000 ppm $MgCO_3$ and 1000 ppm MAP with 5 and 20 ppm Cu²⁺ or 100 ppm Zn²⁺ added to the simulated wastewater solution. (b) Kinetic modeling of experimental data using the pseudo-2nd order kinetic model for 5 and 20 ppm Cu²⁺ or 100 ppm Zn²⁺.

interaction with the MgCO₃ surface, potentially leading to its passivation against Mg²⁺ dissolution.

Fig. 6 presents the elemental composition of the main metals, Mg, Cu, and Zn, and nonmetal P in the recovered filtered and dried solid precipitate as well as in the filtrate obtained from 20 ppm Cu²⁺ and 100 ppm Zn²⁺ containing wastewater transformation into struvite. Quite remarkably, all of the Zn²⁺ and most of the Cu²⁺ ions were incorporated into the resulting solid precipitate. Mg and P, on the other hand, partitioned between the solid and liquid phases quite differently. In the 20 ppm Cu²⁺ case almost all of the Mg accumulated in the solid phase while P was not adsorbed, consistent with the ion chromatography measurements. In the 100 ppm Zn²⁺ case, Mg partitioned between both the solid and liquid phases whereas P was mostly retained in the solid. Collectively, these data show that small amounts of Cu2+ and Zn2+ ions can not only profoundly affect the formation kinetics of the struvite product but also completely inhibit the PO₄³⁻ (and NH₄⁺) adsorption/reaction on MgCO₃, a phenomenon not routinely observed when MgCl2 was used even at relatively high metal ion concentrations. 29,35,55,56

Solid-phase crystalline characterization of struvite formation products formed using MgCO3. Motivated by the slow adsorption of PO₄³⁻ ions in the presence of Cu²⁺ observed, a range of struvite synthesis experiments were performed with 2, 5, 10 or 20 ppm Cu2+ to analyze the resulting crystalline nature of the precipitate. The XRD results for Cu-struvite in Fig. 7 show that moderate concentrations of Cu2+ (10 and 20 ppm) in the wastewater precursor solution suppress struvite formation, while low concentrations of Cu²⁺ (5 ppm) lead to the onset of the struvite crystallization. In particular, the resulting XRD patterns when 10 and 20 ppm of Cu2+ were used are effectively very similar to those of the MgCO3, as shown in Fig. 7a. 100 ppm of Zn²⁺ also showed formation of the struvite phase after 2 hours but a distinct hopeite (Zn₃(PO₄)₂·4H₂O) crystalline phase after 20 minutes of the reaction as shown in Fig. 7b. This is in good agreement with the pseudo-2nd order kinetics observed for the Zn²⁺ removal from the simulated wastewater solution. The supporting EDS measurements shown in Fig. 8 confirm the presence of Zn²⁺ in the solid phase after 20 min with less P incorporated than after 2 hour synthesis. It can also be seen that no P was

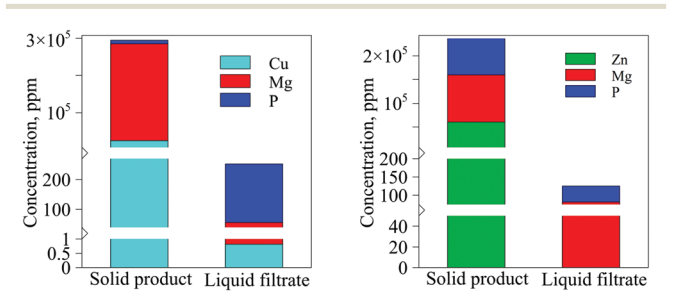


Fig. 6 ICP measured Cu(Zn), Mg and P concentrations in the solid precipitate and the liquid filtrate for 20 ppm Cu²⁺ and 100 ppm Zn²⁺.

Paper

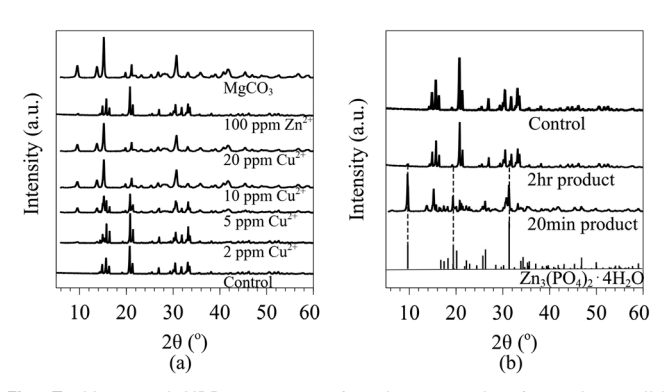


Fig. 7 Measured XRD patterns of various struvite formation solid precipitates using MgCO $_{\rm 3}$ with and without (a) Cu $^{\rm 2+}$ or (b) Zn $^{\rm 2+}$ in the simulated wastewater solution. The control represents struvite formed with no metals added.

incorporated into the reaction product when 20 ppm Cu²⁺ was used while in the 5 ppm Cu2+ case elongated struvite crystals started appearing with dispersed copper.

The nature of copper sites in the solid precipitate is critical in this work as it can suggest potential green struvite fertilizer product biotoxicity. To understand the molecular arrangement of these sites, ambient XANES K-edge studies were conducted to elucidate the coordination for the Cu²⁺ and Zn²⁺ atomic centers incorporated into the synthesized solid precipitate. Fig. 9a shows the 5 ppm and 20 ppm Cu²⁺ near-edge spectra with the references Cu₂O, CuO, and CuSO₄ (aq). The pre-edge feature of Cu₂O which contains linearly coordinated Cu²⁺ is absent in both the 5 and 20 ppm samples. The minor feature at 8977 eV for CuSO₄ is observed

Environmental Science: Water Research & Technology

for both 5 and 20 ppm Cu²⁺. This feature has been previously reported in the literature as the 1s \rightarrow 3d transition.⁵⁷ The lack of a pre-edge feature indicates Cu2+ to be in symmetric coordination, similar to CuO (square planar) and CuSO_{4 (aq)} (elongated octahedral).⁷⁸ The white line of both the 5 and 20 ppm samples aligns with CuO and CuSO₄, indicating that the majority of Cu sites are in the +2 oxidation state (but not in the oxide form). Fig. 9b shows the XANES spectrum for Znstruvite and the reference ZnO spectrum. The shift in the main edge feature which is attributed to $1s \rightarrow 4p^{58}$ indicates distortion from the ZnO structure. The smaller peak following the main edge is attributed to multiple scattering resonance.⁵⁹ The ZnO reference and 100 ppm Zn²⁺ spectra show significant differences, indicating that Zn2+ exists in a disordered phosphate-hydrate phase. 60-62 The XANES spectra bear similarity to that of hopeite (as discussed earlier in the XRD findings), while EXAFS shows that Zn has a distorted octahedral local coordination.

The ambient K-edge EXAFS studies were conducted to elucidate the nearest neighbor information. Table 1 shows the bond length (R), coordination number (N), mean square variation in path length (σ^2), and R factor for the fit. In all three cases, only a single shell is observed, which indicates that the metal centers only have short-range order and show no long-range order given the lack of Me-O-Me bridging bonds. The 5 ppm and 20 ppm Cu²⁺ EXAFS spectra were fitted with N = 4 for equatorial O and N = 2 for axial O bonds. The longer equatorial bond distances were calculated with higher error in the fit compared to the equatorial O bond lengths. The XANES analysis indicates that Cu2+ is coordinated to O in symmetrical coordination and given the

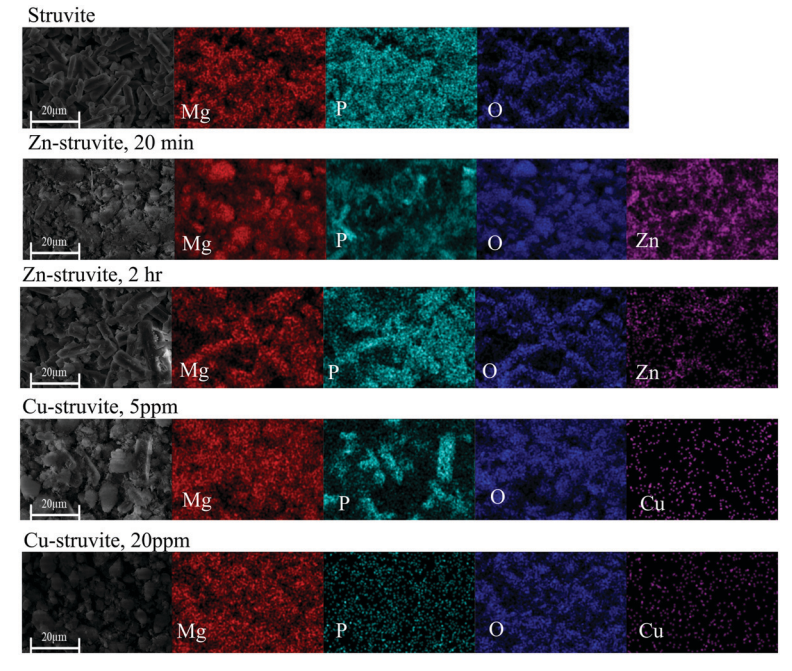


Fig. 8 SEM images together with the elemental EDS maps of various struvite formation solid precipitates using MgCO₃ with and without Cu²⁺ or Zn²⁺ in the simulated wastewater solution.

Environmental Science: Water Research & Technology

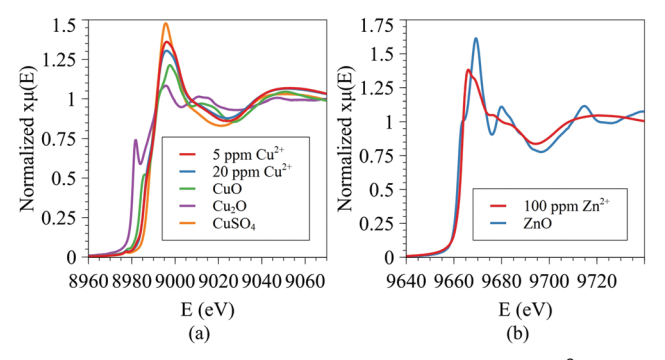


Fig. 9 (a) Cu K-edge XANES spectra for 5 ppm and 20 ppm Cu²⁺ samples with Cu₂O, CuO, and CuSO₄ reference spectra and (b) Zn K-edge XANES spectrum for the Zn sample with the ZnO reference spectrum.

elongated Cu-O axial bond it is difficult to determine whether the exact coordination is square planar or elongated octahedral. In the case of 100 ppm Zn²⁺, three models were evaluated. The lowest R factor was found to be in Zn^{2+} coordinated to 4 equatorial O and 2 axial O atoms. Between the N=4 model and the N=4 and 2 model the R factor variation is minor and thus, it is difficult to discriminate between the models without further experimental evidence to prove the exact Zn2+ coordination. However, the EXAFS analysis conclusively proves that all transition metal centers are highly isolated in the struvite structure, which is in contrast with the work done using MgCl2 where polymeric Zn2+ was detected.32

Furthermore, EXAFS analysis showed that copper metal centers exist in a disordered form, which agrees with previous reports.33 A previous study demonstrated that particle size effects exist (micro vs. nano) for Cu²⁺ uptake in plants. The study concluded that microparticles inhibited root growth at a higher level compared to nanoparticles.⁶³ Cu-struvite has been characterized as a potential slow-release fertilizer for micronutrient delivery in a previous report⁶⁴ with copper precipitation occurring as both phosphate and hydroxide phases. It was shown that organic acids secreted by root systems assisted in forming soluble Cu²⁺ species in soil that can be readily taken up by the plants. The data shown in Fig. 10 suggest that Cu2+ species are coordinated differently from those of bulk corresponding oxides (Cu2O and CuO) and exhibit octahedral coordination.⁶⁵

The Zn-struvite showed minor additional peaks for the 2 hour product in the XRD data in Fig. 7, notably at 9.76° which may be attributed to Zn₃(PO₄)₂·4H₂O (hopeite) minor product formation along with the struvite major product. As shown by the EXAFS analysis, the Zn²⁺ metal centers exist without longrange order, indicating an amorphous (or disordered) phase.⁶¹ Struvite formed using MgCl2 has also been shown to have similar Zn²⁺ centers at low zinc concentrations.³²

Struvite effects on biomass

Soil microbial biomass carbon (SMBC) response to the struvite synthesis solid precipitate. The preceding discussion suggests that the synthesized precipitate contains both Zn and Cu when using solid MgCO3 as a magnesium source. Soil microbial biomass is often used as an early indicator of soil quality changes and is susceptible to changes in the soil environment and soil environmental practices. 66,67 The rapid increase in biomass over the first 12 days (Fig. 11a) of incubation in the struvite treatment indicates that it is a suitable N source for aerobic microbial growth and the release of CO2.68 The initial increase observed in both the struvite and struvite obtained from simulated wastewater solutions containing 100 ppm Zn²⁺ biomass is consistent with N fertilization in a nitrogen-limited environment. The lack of increased biomass in the struvite from 20 ppm Cu²⁺ containing wastewater indicates an overall growth-limiting effect that can be associated with copper toxicity and is consistent with previous studies that have shown copper inhibition of soil microbial biomass C.69,70 After 12 days of incubation the struvite treatment resulted in an overall reduction of the biomass compared to the control. This reduction could be due to the rapid depletion of O2 caused by increased respiration resulting from N fertilization and a transition from consortia dominated by aerobic organisms to anaerobic consortia. However, the biomass continued to increase in the control and struvite made from 100 ppm Zn²⁺ containing wastewater treatments until 28 days followed by a reduction in biomass to the same level as the struvite synthesized from simulated wastewater containing 100 ppm Zn²⁺ at 48 days. The presence of the zinc may have slowed down the growth of the microbial biomass compared to struvite and simply resulted in a delay in the onset of anaerobic conditions. Alternatively, the presence of

Table 1 EXAFS fitting parameters for the reaction products of 1000 ppm MgCO₃ and 1000 ppm MAP in the presence of 5 and 20 ppm Cu²⁺ and 100 ppm Zn²⁺

Sample	Path	N	R (Å)	$\sigma^2 (\mathring{\mathrm{A}}^2)$	R factor (%)
5 ppm Cu ²⁺	Cu-O (eq.)	4	1.940 (0.009)	0.0050 (0.0006)	1.8
	Cu-O (ax.)	2	2.5 (0.1)	0.037 (0.022)	
20 ppm Cu ²⁺	Cu-O (eq.)	4	1.939 (0.090)	0.0058 (0.0005)	1.9
	Cu-O (ax.)	2	2.5 (0.1)	0.035 (0.025)	
100 ppm Zn ²⁺	Zn-O	6	1.967 (0.021)	0.0179 (0.0014)	5.8
	Zn-O	4	1.972 (0.010)	0.0113 (0.0007)	2.1
	Zn-O	4	1.993 (0.010)	0.0098 (0.0006)	1.7
		2	2.27 (0.02)	0.017 (0.004)	

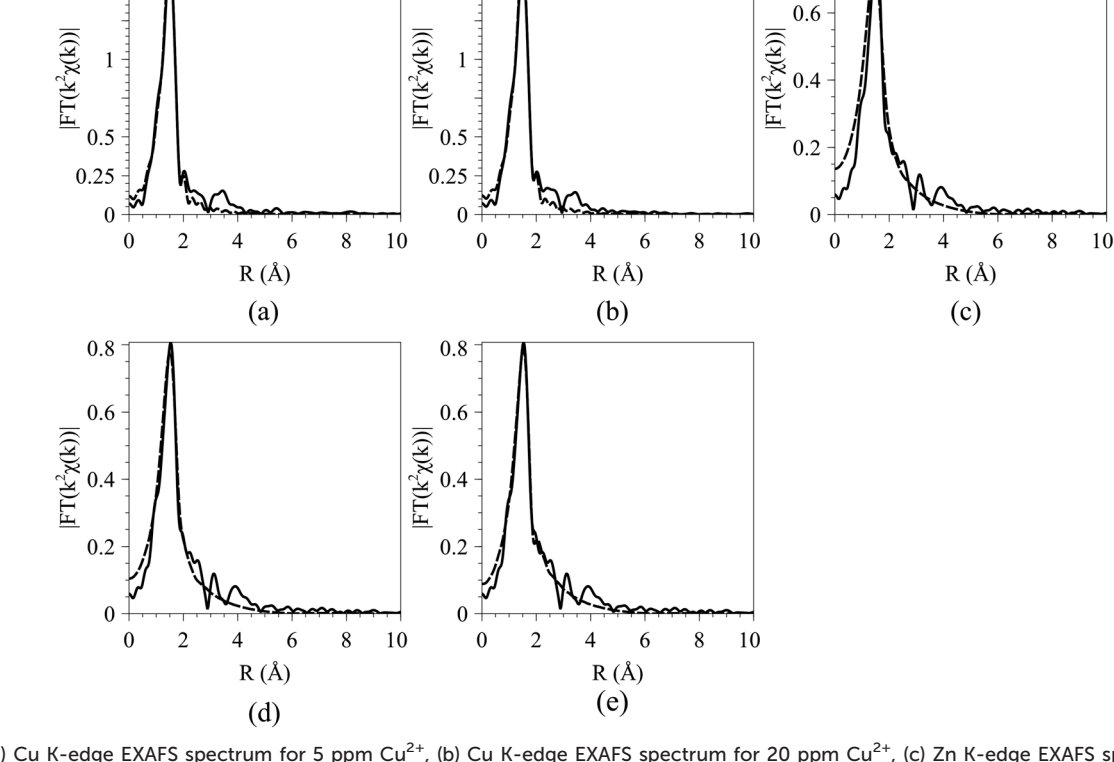
0.8

Paper

1.75

1.5





1.75

1.5

Fig. 10 (a) Cu K-edge EXAFS spectrum for 5 ppm Cu²⁺, (b) Cu K-edge EXAFS spectrum for 20 ppm Cu²⁺, (c) Zn K-edge EXAFS spectrum for 100 ppm Zn^{2+} (fit N=6), (d) Zn K-edge EXAFS spectrum for 100 ppm Zn^{2+} (fit N=4) and (e) Zn K-edge EXAFS spectrum for 100 ppm Zn^{2+} (fit N=4) and 2). The solid line denotes the experimental spectrum, and the dashed line denotes the fitted model.

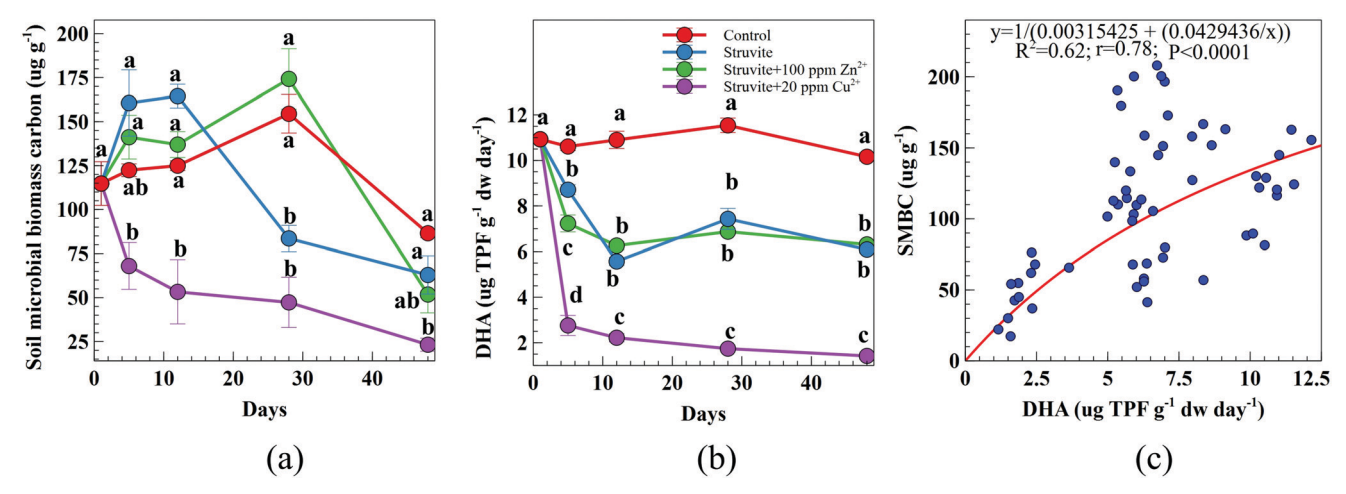


Fig. 11 (a) Soil microbial biomass carbon (SMBC) content and (b) soil DHA activity and (c) the correlation between SMBC and DHA. The best fit is a double reciprocal correlation curve which explains 61.59% of the obtained results. The correlation coefficient (r = 0.78) indicates that there is a strong positive relationship between the SMBC and DHA values.

the zinc may have led to increased alcohol dehydrogenase activity as the consortia became more anaerobic resulting in increased growth in facultative anaerobic organisms. The control treatment was already at a steady state with regard to the N content so there was no increased respiration resulting in a much longer lag time until the onset of anaerobic conditions and the commensurate reduction in anaerobic biomass.

Dehydrogenase activity helps to access the enzymatic activity in the soil and serves as an indicator of microbiological redox systems and is closely correlated with respiratory (aerobic) activity in the soil.⁷¹ Soil dehydrogenase activity was greatly influenced by the addition of N as shown in Fig. 11b. This was evidenced by the significant decrease in DHA throughout the incubation period. The DHA reduction in the struvite and struvite synthesized using 100 ppm Zn²⁺

containing model wastewater is indicative of a transition from aerobic to anaerobic conditions over the first 12 days of incubation and is consistent with the biomass data. The TTC method used to measure DHA is not suited to measure anaerobic dehydrogenase so the level indicated is probably representative of the equilibrium redox state reached after 12 days. Metal concentrations tend to directly affect enzyme activity rather than microbial biomass reduction. The rapid reduction in DHA observed in the struvite synthesized using 20 ppm Cu²⁺ containing wastewater would indicate that there is an overall negative or toxic effect due to the copper. This confirmed previous studies^{72,73} stating inhibition of enzymatic activity in soils by changing the microflora composition and activity of individual enzymes which decreases organic matter decomposition. One possible explanation for the slight increase in DHA in struvite on day 28 may be a result of an increase in pH based on the application of struvite which confirms previous reports that changes in pH of the soil are a frequent effect of struvite application. 14,74 The increased pH has a direct effect on dehydrogenase activity as also reported by other authors. 75

The activity of soil microorganisms strongly depends on the presence of available organic C and N. The lower microbial activity observed in the amendments compared to the control may partly be attributed to the quality as well as the complex interaction of the amendments with the soil.⁷⁶ The alkaline state of the soil makes the initial solubility lower in struvite and other amendments hence did not stimulate quicker mineralization of available soil (phosphorus forms) and a faster growth rate of the soil microorganisms. The lower solubility can be assumed to result in greater immobilization of P compared to the mineralization of the available organic compounds. This resulted in the moderate to low soil microbial-mediated mineralization in struvite and that obtained using 100 ppm Zn²⁺ and 20 ppm Cu²⁺ containing model wastewater as evidenced by the positive correlation between the DHA and SMBC shown in Fig. 11c.

Conclusions and environmental implications. Struvite synthesis using N and P available in wastewater requires a magnesium source which can be either water-soluble MgCl2 or very low water solubility but more available magnesium minerals, including MgCO3. MgCl2 is produced via energydemanding processes while MgCO3 is an abundant mined mineral¹⁰ suggesting that its use can be beneficial for low environmental impact nutrient recovery processes. However, the data presented in this work show that the nature of the complex wastewater needs to be carefully considered before MgCO₃ can be used to substitute MgCl₂. In particular, while solid struvite formed from the simulated wastewater with and without 100 ppm Zn2+, already ppm-level concentrations of Cu²⁺ inhibited the formation of crystalline struvite. The likely mechanism for this phenomenon was surface adsorption of Cu²⁺ ions on MgCO₃ which inhibited Mg²⁺ ion release from the surface. This is an interesting observation and the exact mechanism is a subject of a detailed surface science study.

Notably, this negative effect of the Cu²⁺ ions on the formation of struvite was not observed when MgCl2 was used as a magnesium source for a wide range of Cu2+ ion concentrations.^{29,33,55,56} These surface adsorbed Cu²⁺ sites exhibited a strong effect on soil biota, likely due to being more mobile or soluble. This phenomenon was not observed when 100 ppm Zn²⁺ was present in the simulated wastewater. The Zn-struvite formation proceeded via the formation of a Zn₃(PO₄)₂·4H₂O intermediate in the first ~25 minutes of the reaction which led to a disordered or amorphous Zn local structure in the final product. Notably, in either case, the parent MgCO₃ was a very efficient metal ion adsorbent with both transition metals very efficiently adsorbed and concentrated in the resulting solid under the reaction conditions considered. This suggests that when a more sustainable Mg²⁺ source based on low solubility Mg minerals is considered, due attention needs to be given to the abundance of the particular transition metals in the wastewater.

Author contributions

Karolina Barčauskaitė: investigation and writing the original draft. Donata Drapanauskaitė: investigation. Manoj Silva: visualization, data curation and writing the original draft. Vadim Murzin: investigation. Modupe Doyeni: investigation. Marius Urbonavicius: investigation. Clinton F. Williams: data curation. Skaidrė Supronienė: investigation. Jonas Baltrusaitis: conceptualization, supervision, writing review & editing.

Conflicts of interest

There are no conflicts of interest to declare.

Acknowledgements

This material is based upon work supported by the National Science Foundation under Grant No. CHE 1710120. VM is grateful for financial support from the BMBF project 05K19PXA.

References

- 1 L. Bouwman, K. K. Goldewijk, K. W. Van Der Hoek, A. H. W. Beusen, D. P. Van Vuuren and J. Willems, et al., Exploring global changes in nitrogen and phosphorus cycles in agriculture induced by livestock production over the 1900-2050 period, Proc. Natl. Acad. Sci. U. S. A., 2013, 110(52), 20882-20887, Available from: http://www.pnas.org/content/ 110/52/20882.abstract.
- 2 A. F. Bouwman, L. J. M. Boumans and N. H. Batjes, Estimation of global NH 3 volatilization loss from synthetic fertilizers and animal manure applied to arable lands and grasslands, Global Biogeochem. Cycles, 2002, 16(2), 8.
- 3 J. N. Galloway, J. D. Aber, J. W. Erisman, S. P. Seitzinger, R. W. Howarth and E. B. Cowling, et al., The Nitrogen Cascade, BioScience, 2003, 53(4), 341-356, DOI: 10.1641/ 0006-3568(2003)053[0341:TNC]2.0.CO.

- 4 J. Baltrusaitis, Sustainable Ammonia Production, ACS Sustainable Chem. Eng., 2017, 5(11), 9527-9527.
- 5 D. Cordell, A. Rosemarin, J. J. Schröder and A. L. Smit, Towards global phosphorus security: a systems framework for phosphorus recovery and reuse options, Chemosphere, 2011, **84**(6), 747–758, Available from: sciencedirect.com/science/article/pii/S0045653511001652.
- 6 D. Cordell, I.-O. Drangert and S. White, The story of phosphorus: Global food security and food for thought, Glob. Environ. Change, 2009, 19(2), 292-305.
- 7 H. Zhang, Z. Cao, Q. Shen and M. Wong, Effect of phosphate fertilizer application on phosphorus (P) losses from paddy soils in Taihu Lake Region: I. Effect of phosphate fertilizer rate on P losses from paddy soil, Chemosphere, 2003, 50(6), 695–701.
- 8 L. Mazzei, V. Broll, L. Casali, M. Silva, D. Braga and F. Grepioni, et al., Multifunctional Urea Cocrystal with Combined Ureolysis and Nitrification Inhibiting Capabilities for Enhanced Nitrogen Management, ACS Sustainable Chem. Eng., 2019, 7(15), 13369-13378, DOI: 10.1021/acssuschemeng.9b02607.
- 9 L. Casali, L. Mazzei, O. Shemchuk, L. Sharma, K. Honer and F. Grepioni, et al., Novel Dual-Action Plant Fertilizer and Urease Inhibitor: Urea Catechol Cocrystal. Characterization and Environmental Reactivity, ACS Sustainable Chem. Eng., 2019, 7(2), 2852–2859, DOI: 10.1021/acssuschemeng.8b06293.
- 10 D. Kiani, Y. Sheng, B. Lu, D. Barauskas, K. Honer and Z. Jiang, et al., Transient Struvite Formation during Stoichiometric (1:1) NH4+ and PO43- Adsorption/Reaction on Magnesium Oxide (MgO) Particles, ACS Sustainable Chem. Eng., 2018, 7, 1545-1556.
- 11 L. Sharma, D. Kiani, K. Honer and J. Baltrusaitis, Mechanochemical Synthesis of Ca- and Mg-Double Salt Crystalline Materials Using Insoluble Alkaline Earth Metal Bearing Minerals, ACS Sustainable Chem. Eng., 2019, 7, 6802-6812.
- 12 K. S. Le Corre, E. Valsami-Jones, P. Hobbs and S. A. Parsons, Phosphorus Recovery from Wastewater by Struvite Crystallization: A Review, Crit. Rev. Environ. Sci. Technol., 2009, 39(6), 433-477.
- 13 D. Kiani, M. Silva, Y. Sheng and J. Baltrusaitis, Experimental Insights into the Genesis and Growth of Struvite Particles on Low-Solubility Dolomite Mineral Surfaces, J. Phys. Chem. C, 2019, **123**(41), 25135–25145, DOI: 10.1021/acs.jpcc.9b05292.
- 14 P. J. Talboys, J. Heppell, T. Roose, J. R. Healey, D. L. Jones and P. J. A. Withers, Struvite: a slow-release fertiliser for sustainable phosphorus management?, Soil, 2016, **401**(1), 109-123, DOI: 10.1007/s11104-015-2747-3.
- 15 M. Silva, K. Barcauskaite, D. Drapanauskaite, H. Tian, T. Bučko and J. Baltrusaitis, Relative Humidity Facilitated Urea Particle Reaction with Salicyclic Acid: A Combined in situ Spectroscopy and DFT Study, ACS Earth Space Chem., 2020, 4(7), 1018-1028.
- 16 P. Xia, X. Wang, X. Wang, J. Song, H. Wang and J. Zhang, et al., Struvite crystallization combined adsorption of phosphate and ammonium from aqueous solutions by mesoporous MgO-loaded diatomite, Colloids Surf., A, 2016, 506, 220-227, Available from: http://www.sciencedirect. com/science/article/pii/S092777571630440X.

- 17 M. Quintana, E. Sánchez, M. F. Colmenarejo, J. Barrera, G. García and R. Borja, Kinetics of phosphorus removal and struvite formation by the utilization of by-product magnesium oxide production, Chem. 2005, 111(1), 45-52.
- 18 P. Stolzenburg, A. Capdevielle, S. Tevchené and B. Biscans, Struvite precipitation with MgO as a precursor: Application to wastewater treatment, Chem. Eng. Sci., 2015, 133, 9-15, Available from: http://www.sciencedirect.com/science/article/ pii/S0009250915001797.
- 19 B. Lu, D. Kiani, W. Taifan, D. Barauskas, K. Honer and L. Zhang, et al., Spatially Resolved Product Speciation during Struvite Synthesis from Magnesite (MgCO 3) Particles in Ammonium (NH 4 +) and Phosphate (PO 4 3-) Aqueous Solutions, J. Phys. Chem. C, 2019, 123(14), 8908-8922, DOI: 10.1021/acs.jpcc.8b12252.
- 20 E. Kirinovic, A. R. Leichtfuss, C. Navizaga, H. Zhang, J. D. S. Christus and J. Baltrusaitis, Spectroscopic and microscopic identification of the reaction products and intermediates during the struvite (MgNH4PO4·6H2O) formation from magnesium oxide (MgO) and magnesium carbonate (MgCO3) microparticles, ACS Sustainable Chem. Eng., 2017, 5(2), 1567-1577.
- 21 J. Hövelmann and C. V. Putnis, In Situ Nanoscale Imaging of Struvite Formation during the Dissolution of Natural Brucite: Implications for Phosphorus Recovery from Wastewaters, Environ. Sci. Technol., 2016, 13032-13041, DOI: 10.1021/acs.est.6b04623.
- 22 J. Pesonen, P. Myllymäki, S. Tuomikoski, G. Vervecken, T. Hu and H. Prokkola, et al., Use of Calcined Dolomite as Chemical Precipitant in the Simultaneous Removal of Ammonium and Phosphate from Synthetic Wastewater and from Agricultural Sludge, ChemEngineering, 2019, 3(2), 40.
- 23 L. Chen, C. H. Zhou, H. Zhang, D. S. Tong, W. H. Yu and H. M. Yang, et al., Capture and recycling of ammonium by dolomite-aided struvite precipitation and thermolysis, Chemosphere, 2017, 187, 302-310.
- 24 V. K. Gupta, I. Ali, T. A. Saleh, A. Nayak and S. Agarwal, Chemical treatment technologies for waste-water recycling -An overview, RSC Adv., 2012, 2(16), 6380-6388.
- 25 R. Canziani, Spinosa L. Sludge from wastewater treatment plants, in Industrial and Municipal Sludge: Emerging Concerns and Scope for Resource Recovery, Elsevier, 2019, pp. 3-30.
- 26 A. G. Jiries, F. M. Al Nasir and F. Beese, Pesticide and heavy metals residue in wastewater, soil and plants in wastewater disposal site near Al-Lajoun Valley, Water, Air, Soil Pollut., 2002, 133(1-4), 97-107.
- 27 C. Wang, X. Hu, M. L. Chen and Y. H. Wu, Total concentrations and fractions of Cd, Cr, Pb, Cu, Ni and Zn in sewage sludge from municipal and industrial wastewater treatment plants, J. Hazard. 2005, **119**(1-3), 245-249.
- 28 T. Zubala, M. Patro and P. Boguta, Variability of zinc, copper and lead contents in sludge of the municipal stormwater treatment plant, Environ. Sci. Pollut. Res., 2017, 24(20), 17145-17152.

- 29 S. Muryanto and A. P. Bayuseno, Influence of Cu2+ and Zn2+ as additives on crystallization kinetics and morphology of struvite, Powder Technol., 2014, 253, 602-607.
- 30 M. Ronteltap, M. Maurer and W. Gujer, The behaviour of pharmaceuticals and heavy metals during struvite precipitation in urine, Water Res., 2007, 41(9), 1859-1868.
- 31 A. Uysal, Y. D. Yilmazel and G. N. Demirer, The determination of fertilizer quality of the formed struvite from effluent of a sewage sludge anaerobic digester, J. Hazard. Mater., 2010, 181(1-3), 248-254.
- 32 A. A. Rouff and K. M. Juarez, Zinc Interaction with Struvite During and After Mineral Formation, Environ. Sci. Technol., 2014, 48(11), 6342-6349.
- 33 A. A. Rouff, M. V. Ramlogan and A. Rabinovich, Synergistic Removal of Zinc and Copper in Greenhouse Waste Effluent by Struvite, ACS Sustainable Chem. Eng., 2016, 4(3), 1319-1327.
- 34 C. Tang, Z. Liu, C. Peng, L.-Y. Chai, K. Kuroda and M. Okido, et al., New insights into the interaction between heavy metals and struvite: Struvite as platform for heterogeneous nucleation of heavy metal hydroxide, Chem. Eng. J., 2019, 365, 60-69, Available from: https://linkinghub.elsevier. com/retrieve/pii/S1385894719302578.
- 35 C. Peng, L. Chai, C. Tang, X. Min, Y. Song and C. Duan, et al., Study on the mechanism of copper-ammonia complex decomposition in struvite formation process and enhanced ammonia and copper removal, J. Environ. Sci., 2017, 51, 222-233, Available from: https://linkinghub.elsevier.com/ retrieve/pii/S100107421630242X.
- 36 N. Ahmed, S. Shim, S. Won and C. Ra, Struvite recovered from various types of wastewaters: Characteristics, soil leaching behaviour, and plant growth, Land Degrad. Dev., 2018, **29**(9), 2864-2879.
- 37 S. K. Gupta, S. Roy, M. Chabukdhara, J. Hussain and M. Kumar Risk of metal contamination in agriculture crops by reuse of wastewater: An ecological and human health risk perspective, in Water Conservation, Recycling and Reuse: Issues and Challenges, Springer Singapore, 2019, pp. 55-79.
- 38 T. Cai, S. Y. Park and Y. Li, Nutrient recovery from wastewater streams by microalgae: Status and prospects, Renewable Sustainable Energy Rev., 2013, 19, 360-369, Available from: http://www.sciencedirect.com/science/article/ pii/S1364032112006429.
- 39 W. A. Caliebe, V. Murzin, A. Kalinko and M. Görlitz, Highflux XAFS-beamline P64 at PETRA III, AIP Conf. Proc., 2019, 060031, American Institute of Physics Inc.
- 40 B. Ravel and M. Newville, ATHENA, ARTEMIS, HEPHAESTUS: Data analysis for X-ray absorption spectroscopy using IFEFFIT, J. Synchrotron Radiat., 2005, 537-541.
- 41 M. Newville, EXAFS analysis using FEFF and FEFFIT, J. Synchrotron Radiat., 2001, 8(2), 96-100.
- 42 A. Ankudinov and J. Rehr, Relativistic calculations of spindependent x-ray-absorption spectra, Phys. Rev. B: Condens. Matter Mater. Phys., 1997, 56(4), R1712-R1716.
- 43 L. E. Casida, D. A. Klein and T. Santoro, Soil dehydrogenase activity, Soil Sci., 1964, 98, 371-376.

- 44 E. D. Vance, P. C. Brookes and D. S. Jenkinson, An extraction method for measuring soil microbial biomass C, Soil Biol. Biochem., 1987, 19(6), 703-707.
- 45 J. Wu, A. G. O'donnell, Z. L. He and J. K. Syers, Fumigationextraction method for the measurement of soil microbial biomass-S, Soil Biol. Biochem., 1994, 26(1), 117-125.
- 46 S. Azizian, Kinetic models of sorption: A theoretical analysis, J. Colloid Interface Sci., 2004, 276(1), 47-52.
- 47 W. Rudzinski and W. Plazinski, Kinetics of solute adsorption at solid/solution interfaces: A theoretical development of the empirical pseudo-first and pseudo-second order kinetic rate equations, based on applying the statistical rate theory of interfacial transport, J. Phys. Chem. B, 2006, 110(33), 16514-16525.
- 48 W. Rudzinski and W. Plazinski, Studies of the kinetics of solute adsorption at solid/solution interfaces: On the possibility of distinguishing between the diffusional and the surface reaction kinetic models by studying the pseudo-firstorder kinetics, J. Phys. Chem. C, 2007, 111(41), 15100-15110.
- A. Priharyoto Bayuseno, D. S. Perwitasari, S. Muryanto, M. 49 Tauviqirrahman and J. Jamari, Kinetics and morphological characteristics of struvite (MgNH 4 PO 4 .6H 2 O) under the influence of maleic acid, Heliyon, 2017, e03533.
- M. S. Rahaman, N. Ellis and D. S. Mavinic, Effects of various process parameters on struvite precipitation kinetics and subsequent determination of rate constants, Water Sci. Technol., 2008, 57(5), 647-654.
- 51 F. Meshkani and M. Rezaei, Facile synthesis of nanocrystalline magnesium oxide with high surface area, Powder Technol., 2009, 196(1), 85-88.
- M. A. Treto-Suárez, J. O. Prieto-García, Á. Mollineda-Trujillo, 52 E. Lamazares, Y. Hidalgo-Rosa and K. Mena-Ulecia, Kinetic study of removal heavy metal from aqueous solution using the synthetic aluminum silicate, Sci. Rep., 2020, 10(1), 1-12.
- 53 W. Peng, H. Li, Y. Liu and S. Song, A review on heavy metal ions adsorption from water by graphene oxide and its composites, J. Mol. Liq., 2017, 230, 496-504.
- 54 X. Liu, K. Song, W. Liu, Y. Xiong, Y. Xu and Z. Shi, et al., Removal and recovery of Pb from wastewater through a reversible phase transformation process between nanoflower-like Mg(OH) 2 and soluble Mg(HCO 3) 2, Environ. Sci.: Nano, 2019, 6(2), 467-477.
- D. S. Perwitasari, S. Muryanto, J. Jamari and A. P. Bayuseno, Kinetics and morphology analysis of struvite precipitated from aqueous solution under the influence of heavy metals: Cu2+, Pb2+, Zn2+, J. Environ. Chem. Eng., 2018, 6(1), 37-43.
- 56 H. Huang, B. Li, J. Li, P. Zhang, W. Yu and N. Zhao, et al., Influence of process parameters on the heavy metal (Zn2+, Cu2+ and Cr3+) content of struvite obtained from synthetic swine wastewater, Environ. Pollut., 2019, 245, 658-665.
- C. Angelici, F. Meirer, A. M. J. van der Eerden, H. L. Schaink, A. Goryachev and J. P. Hofmann, et al., Ex Situ and Operando Studies on the Role of Copper in Cu-Promoted SiO2-MgO Catalysts for the Lebedev Ethanol-to-Butadiene Process, ACS Catal., 2015, 5(10), 6005-6015.

- 58 H. C. Wang, Y. L. Wei, Y. W. Yang and J. F. Lee, XAS study of Zn-doped Al2O3 after thermal treatment, J. Electron Spectrosc. Relat. Phenom., 2005, 817-819.
- 59 W. E. Taifan, Y. Li, J. P. Baltrus, L. Zhang, A. I. Frenkel and J. Baltrusaitis, Operando Structure Determination of Cu and Zn on Supported MgO/SiO 2 Catalysts during Ethanol Conversion to 1,3-Butadiene, ACS Catal., 2019, 9(1), 269-285, DOI: 10.1021/acscatal.8b03515.
- 60 A. Whitaker, The crystal structure of hopeite, Zn 3 (PO 4) 2 .4H 2 O, Acta Crystallogr., Sect. B: Struct. Crystallogr. Cryst. Chem., 1975, 31(8), 2026-2035.
- 61 N. Sato and T. Minami, State analysis related to zinc and manganese components in hopeite crystals of zinc phosphate films by XANES and EXAFS, J. Mater. Sci., 1989, 24(12), 4419-4422.
- 62 E. Castorina, E. D. Ingall, P. L. Morton, D. A. Tavakoli and B. Lai, Zinc K-edge XANES spectroscopy of mineral and organic standards, J. Synchrotron Radiat., 2019, 26(4), 1302-1309.
- 63 W. Du, W. Tan, Y. Yin, R. Ji, J. R. Peralta-Videa and H. Guo, et al., Differential effects of copper nanoparticles/microparticles in agronomic and physiological parameters of oregano (Origanum vulgare), Sci. Total Environ., 2018, 618, 306-312.
- 64 H. Arslanoglu, Adsorption of micronutrient metal ion onto struvite to prepare slow release multielement fertilizer: Copper(II) doped-struvite, Chemosphere, 2019, 217, 393-401.
- 65 D. M. Pickup, I. Ahmed, V. FitzGerald, R. M. Moss, K. M. Wetherall and J. C. Knowles, et al., X-ray absorption spectroscopy and high-energy XRD study of the local environment of copper in antibacterial copper-releasing degradable phosphate glasses, J. Non-Cryst. Solids, 2006, 352(28-29), 3080-3087.
- 66 P. R. Hargreaves, P. C. Brookes, G. J. S. Ross and P. R. Poulton, Evaluating soil microbial biomass carbon as an indicator of long-term environmental change, Soil Biol. Biochem., 2003, 35(3), 401-407.
- 67 Y. Xu, H. Tang, X. Xiao, W. Li, C. Li and G. Sun, et al., Effects of long-term fertilization management practices on

- soil microbial carbon and microbial biomass in paddy soil at various stages of rice growth, Rev. Bras. Cienc. Solo, 2018, 42, DOI: 10.1590/18069657rbcs20170111.
- 68 Effects of heavy metals on soil microbial community -IOPscience.
- 69 Y. Xie, J. Fan, W. Zhu, E. Amombo, Y. Lou and L. Chen, et al., Effect of Heavy Metals Pollution on Soil Microbial Diversity and Bermudagrass Genetic Variation, Front. Plant Sci., 2016, 7, 755.
- 70 Y. P. Wang, J. Y. Shi, H. Wang, Q. Lin, X. C. Chen and Y. X. Chen, The influence of soil heavy metals pollution on soil microbial biomass, enzyme activity, and community composition near a copper smelter, Ecotoxicol. Environ. Saf., 2007, 67(1), 75-81.
- 71 A. Wolinska and Z. Stepniewsk, Dehydrogenase Activity in the Soil Environment, Dehydrogenases, 2012.
- 72 A. Łukowski and D. Dec, Influence of Zn, Cd, and Cu fractions on enzymatic activity of arable soils, Environ. Monit. Assess., 2018, 190(5), 278.
- 73 S. Chaperon and S. Sauvé, Toxicity interaction of metals (Ag, Cu, Hg, Zn) to urease and dehydrogenase activities in soils, Soil Biol. Biochem., 2007, 39(9), 2329-2338.
- 74 M. Szymá Nska, E. Szara, A. W. As, T. Sosulski, G. W. P. Van Pruissen and R. L. Cornelissen, Struvite-An Innovative Fertilizer from Anaerobic Digestate Produced in a Bio-Refinery, Energies, 2019, 12(2), 296.
- 75 C. Quilchano and T. Marañón, Dehydrogenase activity in Mediterranean forest soils, Biol. Fertil. Soils, 2002, 35(2), 102-107.
- 76 S. Bachmann, M. Gropp and B. Eichler-Löbermann, Phosphorus availability and soil microbial activity in a 3 year field experiment amended with digested dairy slurry, Biomass Bioenergy, 2014, 70, 429-439.
- 77 M. Silva and J. Baltrusaitis, Environ. Sci.: Water Res. Technol., 2020, 6, 3178-3194.
- 78 M. Silva, V. Murzin, L. Zhang, J. Baltrus and J. Baltrusaitis, Environ. Sci.: Nano, 2020, 7, 3482-3496.